# The brain's resting-state activity is shaped by synchronized cross-frequency coupling of neural oscillations

**Esther Florin**[*] and **Sylvain Baillet**[*]

[*]McConnell Brain Imaging Center, Montreal Neurological Institute, McGill University, Montreal, 3801 University St, QC, H3A 2B4, Canada

## Abstract

Functional imaging of the resting brain consistently reveals broad motifs of correlated blood oxygen level dependent (BOLD) activity that engage cerebral regions from distinct functional systems. Yet, the neurophysiological processes underlying these organized, large-scale fluctuations remain to be uncovered. Using magnetoencephalography (MEG) imaging during rest in 12 healthy subjects we analyse the resting state networks and their underlying neurophysiology. We first demonstrate non-invasively that cortical occurrences of high-frequency oscillatory activity are conditioned to the phase of slower spontaneous fluctuations in neural ensembles. We further show that resting-state networks emerge from synchronized phase-amplitude coupling across the brain. Overall, these findings suggest a unified principle of local-to-global neural signaling for long-range brain communication.

## Keywords

resting state; phase-amplitude coupling; neural dynamics; neural networks and communication

## 1 Introduction

Over the past 15 years, there has been considerable interest in studying the resting activity of the human brain, particularly with functional magnetic resonance imaging (fMRI) (Raichle, 2011). One remarkable property of spontaneous cerebral activity is that it consistently segregates in resting-state networks (RSN), which coincide anatomically with the major functional systems of the brain (Biswal et al., 2010). Consequently, studies suggest that RSN provide insight into the large-scale mechanisms of healthy and impaired neural communication (Buckner et al., 2005; Tomasi and Volkow, 2012).

Yet, our current understanding of the neurophysiological mechanisms underlying these large-scale fluctuations remains elusive (Leopold and Maier, 2012; Smith, 2012).

Corresponding author: Sylvain Baillet, McConnell Brain Imaging Centre, Montreal Neurological Institute, McGill University, 3801 University St, Montreal, QC, H3A 2B4, Canada, sylvain.baillet@mcgill.ca, Phone: +1 514 398 5469.

Simultaneous BOLD and electrophysiology recordings in the visual cortex of monkeys report that gamma activity of the local field potentials (LFP) is the main electrophysiological basis of the BOLD signal (Logothetis et al., 2001; Shmuel and Leopold, 2008). These local results cannot resolve how the large-scale connectivity across the whole brain of the resting state is generated. Human magnetoencephalography (MEG) of the whole brain emphasized the contribution of alpha and beta oscillatory signals for the generation of the RSNs (Brookes et al., 2011; Pasquale et al. 2010). This conforms well with findings that low-frequency oscillations coordinate long-range communication (Stein, Chiang, and König, 2000). However, these MEG findings do not align entirely with the role of gamma oscillations in local neural activity (Buzsáki and Wang, 2012) and as counterparts of BOLD signaling (Logothetis et al., 2001).

Cross-frequency coupling, in particular phase-amplitude coupling, has been attributed an important role for communication between brain areas (Canolty et al., 2006; Canolty and Knight, 2010; Jensen and Colgin, 2007). Therefore cross-frequency coupling between a low-frequency phase and gamma activity may be an ideal candidate for the communication in the RSN. Based on these previous results we here test two hypotheses. First, interregional correlated fluctuations during rest are regulated by the coupling between the phase of slow-frequency activity and the amplitude of high-frequency oscillations. Second, this mechanism defines the principal modes of resting-state connectivity.

To test these hypotheses we use a model (megPAC), which consists of the interpolated gamma amplitude at key-events of the strongest coupling low-frequency phase. The rationale for this signal model posits that the excitability cycles of local populations need to be synchronized to form a network. Therefore, a core hypothesis is that the phases of local low-frequency oscillations emerging from communicating brain regions need to be time-locked, with no phase delay. This condition is based on evidence from the small-world architecture of brain connectivity suggesting that cortical or subcortical hubs facilitate synchronization of distant oscillatory activity with zero-lag (i.e. with no phase delay) (Haider et al., 2006). Population excitability cycles commonly occur at lower frequencies (Osipova, Hermes, and Jensen, 2008). Therefore this slower oscillatory rhythm may provide a gating mechanism that time-marks the operations of local circuits, revealed by bursts of higher-frequency activity (Buzsáki and Draguhn, 2004; Buzsáki and Wang, 2012; Lakatos et al., 2005). Along this hypothesis, an additional condition to network formation requires coherent high-frequency oscillations between regions: this would facilitate local post-synaptic integration and spiking activity to occur in concert amongst network elements. Previous observations suggest that high-frequency bursts are preferentially occurring about the trough of the low-frequency phase cycles of local field potentials (Canolty et al., 2006).

Consequently, we confirm and extend non-invasively in healthy participants for the entire brain previous observations of local phase-amplitude coupling (PAC) (Canolty et al., 2006; Osipova, Hermes, and Jensen, 2008). We show that the oscillatory components conditioning the preferred timing of high-frequency activity through PAC span a relatively wide low-frequency range: from delta (2-4 Hz), theta (4-8 Hz), to alpha (8-12 Hz) bands. With these results we demonstrate that PAC contributes to the network connectivity, thereby delivering a principle for global communication across the brain at rest.

## 2 Materials and Methods

Note that most data preprocessing and MEG source imaging was performed using Brainstorm (Tadel et al., 2011). Brainstorm is an open-source software, freely available to the academic community (http://neuroimage.usc.edu/brainstorm/). All implementation details are therefore readily documented and can be verified in Brainstorm's code.

### Data Acquisition

The study was approved by the local ethics committee, in accordance with the Declaration of Helsinki. 12 healthy, right-handed subjects (4 females, 8 males; age range: 21-41 y.o.) were recruited to participate in the study and all subjects gave informed consent.

The participants were tested for possible magnetic artifacts in a short preliminary MEG run. Subjects preparation consisted of taping 3 to 4 head-positioning coils on the subject's scalp. The positions of the coils were measured relative to the subject's head using a 3-D digitizer system (Polhemus Isotrack). To facilitate anatomical registration with MRI, about 100 additional scalp points were also digitized. One pair of electrodes was positioned and taped across the participants' chest (one above the inferior extremity of the left rib cage and one over the right clavicle) to capture electrocardiographic (ECG) activity synchronized with the MEG traces. Similarly, one pair of electrodes was attached above and below one eye to detect eye-blinks and large saccades (EOG).

5 subjects were measured in seated position with the Elekta-Neuromag VectorView 306-channel system with a sampling rate of 2000 Hz (0.03 Hz high-pass online filter, 660 Hz anti-aliasing low-pass online filter); 7 subject were measured in seated position using the 275-channel VSM/CTF system with a sampling rate of 2400 Hz (no high-pass filter, 660 Hz anti-aliasing online low-pass filter). Magnetic shielding was provided by magnetically-shielded rooms (MSR) with full 3-layer passive shielding for the CTF/VSM system, and single-layer shielding with Maxfilter active flux-compensation for the Elekta-Neuromag system. The combination of the two recording systems should not influence our results, because all calculations and combination of the results are performed at the source level. Moreover for task related studies it was shown that the different MEG systems yield essentially identical results (Weisend et al., 2007).

At the beginning of each MEG run, the location of the subject's head within the MEG helmet was measured by energizing the head-positioning coils, following standard procedures. For each subject, between 5 and 30 minutes (20 minutes on average for the subject group) of MEG data were acquired, during an average of 5 runs of 2 to 10-minute duration. The only instruction given to the participants was to keep their eyes open and to relax without falling asleep.

A 2-minute empty-room recording, with the same acquisition parameters, and with no subject present in the MSR, was used to capture some of the sensor and environmental noise statistics, which were used in the source estimation process, as explained below.

For subsequent cortically-constrained MEG source analysis, a T1-weighted MRI acquisition of the cerebrum was obtained from each participant either at least one month before the MEG session or afterwards.

## Data Pre-processing

MEG traces were pre-processed to verify data quality and to reduce contamination from artifacts (cardiac, eye movements and blinks, environmental noise). Data from the Elekta-Neuromag system were preprocessed using signal-space-separation (SSS) (Taulu, Kajola, and Simola, 2004), as implemented in the Maxfilter noise reduction system from Elekta-Neuromag. Default SSS settings were used: orders of spherical harmonic expansions for the inner and outer source models were 8 and 3, respectively. Data from the CTF/VSM system were corrected with the manufacturer's 3rd order gradient compensation system (no parameter setting required). The projectors obtained were propagated to the corresponding MEG source imaging operator.

All recordings were visually inspected to detect segments contaminated by head movements or remaining environmental noise sources, which were discarded from subsequent analysis. Heart and eye movement/blink contaminations were attenuated by designing signal-space projections (SSP) from selected segments of data about each artifactual event (Nolte and Curio, 1999). Using Brainstorm's ECG and EOG detection functionality (Tadel et al., 2011). heartbeat events were automatically detected at the R peak of the ECG's QRS complex, and eye blink events were determined automatically at the peaks of the EOG traces. Projectors were defined using principal component analysis (PCA) of these data segments filtered between 10 and 40 Hz (for heartbeats) or 1.5 and 15 Hz (for eye blinks) in a 160-ms time window centered about the heartbeat event, or 400 ms around the eye blink event. The principal components that best captured the artifact's sensor topography were manually selected as the dimension against which the data was orthogonally projected away from, also using the routines available in Brainstorm. Note that in most subjects, the first principal component was sufficient to attenuate artifact contamination. The projectors obtained for each subject were propagated to the corresponding MEG source imaging operator as explained below. Powerline contamination (main and harmonics) was reduced by complex match filtering with 1-Hz resolution bandwidth for sinusoidal removal, also available in Brainstorm. The pre-processed data were resampled at 1000 Hz, using the polyphase filter implementation from Matlab (The Mathworks, MA, USA) with default parameters.

The scalp and cortical surfaces were extracted from the MRI volume data. A surface triangulation was obtained for each envelope using the segmentation pipeline available in Brainvisa (Riviere et al., 2009) (http://brainvisa.info), with default parameter settings and subsequently imported into Brainstorm. The individual high-resolution cortical surfaces (about 75,000 vertices per surface) were down-sampled to about 15,000 triangle vertices (also with a Brainstorm process) to serve as image supports for MEG source imaging.

## MEG Source Imaging

Forward modeling of neural magnetic fields was performed using the overlapping-sphere technique implemented in Brainstorm (Huang, Mosher, and Leahy, 1999). In this method,

one sphere is automatically adjusted locally to the individual scalp surface under each magnetic sensor to compute the corresponding lead field analytically. This method has been shown to provide the best trade-off between modeling precision and numerical accuracy (Huang, Mosher, and Leahy, 1999). The lead-fields were computed from elementary current dipoles distributed perpendicularly to the cortical surface from each individual (Baillet, Mosher, and Leahy, 2001).

MEG source imaging was performed by linearly applying the weighted-minimum norm operator **W** onto the preprocessed data:

$$\mathbf{W}=\mathbf{A}^T\left(\mathbf{A}\mathbf{A}^T+\lambda\mathbf{C}\right)^{-1} \quad (1)$$

**A** is the gain matrix from the forward solution and **C** the spatial covariance of the noise in the recordings. The empirical estimate of **C** was obtained from the empty-room recording described above (Baillet, Mosher, and Leahy, 2001). $\lambda$ is a scalar regularization parameter. The weights of the imaging operator attenuate the decrease of signal-to-noise ratio between superficial and deeper cortical sources, and between tangential and radially-oriented sources with respect to each of the individual spheres.

As mentioned before, the data were projected away from the spatial components of artifact contaminants. For consistency between the projected data and the model of their generation by cortical sources, the forward operator was itself projected away from the same contaminants using the same projector as for the MEG data. This procedure is automatically verified and applied in Brainstorm.

### Phase-Amplitude Coupling

An analytic measure of cross-frequency coupling was computed from each of the elementary MEG source time series, in each individual subject. For all following computations, all artifact free recordings from each subject were used. They were therefore concatenated in the source space. We used the direct phase-amplitude-coupling (PAC) measure (Özkurt and Schnitzler, 2011), defined as follow:

$$PAC(f_\varphi, f_a)=\frac{1}{\sqrt{N}}\frac{\left|\sum\limits_{n=1}^{N}a(n)e^{i\varphi(n)}\right|}{\sqrt{\sum\limits_{n=1}^{N}a(n)^2}}. \quad (2)$$

$N$ is the data length, $n$ a running time sample; $a$ is the signal amplitude at the high frequency $f_a$, $\varphi$ is the signal phase at the low frequency $f_\varphi$. The signal phase and amplitude were computed using the chirplet transform (Mann and Haykin, 1991), following similar methodology as Canolty et al. (2006).

At each of the $\sim$15,000 individual source locations and for each subject, the maximum PAC score was computed from all frequency pairs $(f_\varphi, f_a)$, with $f_\varphi \in [2,48]$ Hz and $f_a \in [80,150]$

Hz. The binning width for $f_\varphi$ was 0.5 Hz from 2 to 12 Hz and 2 Hz from 12 to 48 Hz. The bins of $f_a$ were logarithmicallly spaced. The optimal low frequency phase in terms of largest PAC score with $f_a \in [80, 150]$ Hz was determined at each cortical location:

$$(\hat{f}_\varphi, \hat{f}_a) = \underset{f_\varphi, f_a}{\arg \max} \, PAC(f_\varphi, f_a). \quad (3)$$

### Statistical analysis of Phase-Amplitude Coupling

Because no analytical significance measure is available that takes into account the usual temporal correlation in neural signals, a bootstrapping-based approach is used to generate the distribution of the PAC measure under the null hypothesis H0 of "no PAC and serial correlation of the type found in neural signals". In particular, we generated PAC scores under H0 using the following procedure: For each subject, 100 random time series with $1/f$ characteristics were generated with durations identical to the subject's actual recordings'. The $1/f$ random time series were generated by applying an AR filter to normally distributed random time series (Kasdin, 1995). To evaluate whether the pink noise data is really able to capture the salient autocorrelation structure of the data, we compared autocorrelograms of the amplitude in different frequency ranges in the experimental and noise data and found them to be quite close to each other (summarized e.g. by the half-life of the correlation).

Based on these artificial noise time series, the critical values for significance testing were computed the following way: for each random time series, the PAC value obtained for each low frequency phase $f_\varphi$ and high frequency amplitude $f_a \in [80, 150]$ Hz was calculated in the same manner as for the experimental data times series. From the 100 surrogate repetitions, the value at the 95th quantile of PAC scores for every low/high frequency pair was determined as the significance threshold at $p < 0.05$ for actual recordings with Bonferroni correction (15,000 sources and 429 frequency pairs, using linear interpolation when necessary).

The optimal low frequency for phase $\hat{f}_\varphi$ was classified in one of the typical sub-bands of electrophysiological neural signals: $\delta = [2,4]$ Hz, $\theta = [4,8]$ Hz, $\alpha = [8,12]$ Hz, $\beta = [12,30]$ Hz or $\gamma = [30,48]$ Hz. Every $\hat{f}_\varphi$ value, obtained at all cortical locations, was mapped onto the individual cortical surface from each subject. For group analysis, the resulting individual significant PAC maps were projected onto the Colin27 brain template, using Brainstorm's multilinear registration procedure. The resulting anatomically-registered maps were then averaged across all 12 subjects excluding the non-significant regions and displayed in Fig. 2a.

### Estimation of frequency with maximal power

For every subject at every cortical location we calculated the power spectral density using the fast fourier transform with half overlapping 4096 data-points long Hanning windows. This yielded a frequency resolution of 0.24Hz. We took the maximal frequency from 2-48Hz in accordance to the maximal PAC determination and calculated the difference to the maximal PAC frequency for all sources.

## Generation of Figure 2b

The method used to obtain Figure 2b was akin to that of Canolty et al., 2006 and applied to the source signals at a random selection of cortical locations. First, the troughs at the optimal nesting frequency $\hat{f}_\varphi$ were determined from the signal phase time series $\varphi_n(\hat{f}_\varphi) \in (-\pi, \pi]$ – with $\varphi_n(\hat{f}_\varphi) = \pi$ corresponding to a trough – obtained with chirplets (Mann and Haykin, 1991). Second, the amplitude $a(n, f)$ of the source signals with $f \in [40, 250]$ Hz was determined, also using the chirplet transform. Third, the amplitude time series $a(n, f)$ was z-scored for each frequency bin:

$$\overline{a}(n, f) = \frac{a(n, f) - \langle a(n, f) \rangle}{\tilde{a}(f)}, \quad (4)$$

where $\langle a(f) \rangle$ is the time average of $a(n,f)$, and $\tilde{a}(f)$ is the temporal standard deviation of $a(n,f)$, estimated over all $N$ time samples, for each subject. Fourth, the time-frequency decomposition $(n, f)$ was epoched over the time window of $[-0.5, 0.5]$ s about each of the previously identified phase troughs yielding $(k, n, f)$. The number of epochs $k$ ranged between 2,600 and 24,000 depending on the data length for each subject. Note that due to the data concatenation of the different runs for each subject, there are slight jumps in the data. However, these occur at most 10 times per subject so that their influence should be negligible. Fifth, time-frequency representations of $(k, n, f)$ were averaged across all k epochs as shown in Figure 2b. Sixth, the source signals were also averaged across all k epochs to obtain $\langle a(k, n) \rangle$ the time series shown at the bottom of the time-frequency maps in Figure 2b.

The significance of phase-amplitude coupling in terms of correlated temporal modulations between the high-frequency nested components and the low-frequency nesting oscillations over the epoch time window was determined by evaluating the slope between the event-related average of the broadband cortical time series, conditioned to phase trough events $(\varphi_n(\hat{f}_\varphi = \pi)$, and the average of the time variations $(k, n, f)$ at every frequency bin $f$. The slope coefficient corresponds to the correlation coefficient. To estimate the slope we used an ordinary least square estimate. Using Newey and West, 1987 robust standard errors and the asymptotically normal distribution of the coefficients, we assessed the significance of the slope coefficients. Significance thresholds were set at each frequency bin $f$ at $p < 0.05$, with Bonferroni correction.

## megPAC and control models

From the MEG source signals we generated a signal model to evaluate factors of long-range connectivity between brain regions in the resting-state. The generation of the megPAC signal models is illustrated schematically in Figure 1: the gamma amplitude of the source signal in the [80, 150] Hz was linearly interpolated with Malab's *interp1* function to the time occurrences $t_\varphi$ of the peaks and troughs of the optimal low-frequency phase $\hat{f}_\varphi$ yielding the largest PAC within the [80,150] Hz high-gamma range, as obtained from Eq. 3. The gamma amplitude in the [80, 150] Hz range was obtained from the chirplet transform of the original source signal, as explained above. To compensate for the $1/f$ decrease in signal power, the gamma amplitude was calculated at logarithmically-spaced frequency bins and each

temporal variation at each bin was z-transformed. Therefore the values of the mean and standard deviation were taken over the entire individual recording ($N$ time samples) for each frequency bin. An estimation of the signal amplitude in the [80, 150] Hz range was obtained from averaging over all frequency bins in that range. The resulting megPAC ($t_\phi$) values were subsequently downsampled to 10 Hz after applying an anti-aliasing filter.

To verify the validity of the megPAC model, we generated three alternative models:

1. We investigated whether identifying the optimal coupling frequency $\hat{f}_\phi$ at each cortical location was critical to the extraction of resting-state networks. We therefore generated another signal model following the same approach as with the megPAC model, but with a nesting frequency arbitrarily set in the $\theta$ range at 5.4 Hz, for each of the 15,000 tested brain locations, as used by Canolty et al., 2006.

2. We tested whether the identification of certain low-frequency events is essential at all. Therefore we selected random time-points of the gamma amplitude and interpolated between those.

3. We generated 12 sets of random time series with $1/f$ characteristics, which simulated MEG sensor activity. These data sets were source reconstructed with a weighted minimum-norm operator on the Colin27 brain. For these data the optimal PAC frequency and the megPAC model were calculated. This model was used to determine effects in the obtained networks, from the processing pipeline and the sensitivity profile of MEG source imaging.

## Extraction of Resting-State Networks and Statistical Thresholds

The following procedure for extracting resting-state networks as dominant patterns of connectivity between cortical sources was applied to each signal model introduced in the previous section:

1. Projection onto anatomical template: The individual megPAC time series were projected onto the Colin27 cortical surface template (consisting of $N_\upsilon$=15,000 triangle vertices) using the multilinear scaling and registration procedure.

2. Spatial smoothing and signal concatenation: The cortical maps obtained from the megPAC and alternative signal models were spatially smoothed with a non-recursive kernel of 7mm full-width at half maximum applied at the surface of the cortex. The time series of all subjects were concatenated, following previous reports in MEG (Brookes et al., 2011) and fMRI (Smith et al., 2009) RSN analysis.

3. Connectivity matrices: The pairwise correlation coefficients were calculated between the time series taken at each pair of cortical sources, yielding the $N_\upsilon \times N_\upsilon$ array $\bar{C}$ of empirical correlation coefficients.

4. Dimensionality reduction: We conducted the extraction of RSN maps by obtaining the principal spatial modes of $\bar{C}$. To make this operation computationally tractable, each row of $\bar{C}$ was projected orthogonally onto those of $\bar{C}_{1175}$, a subset of 1175 rows from $\bar{C}$ corresponding to cortical locations evenly distributed over the

template cortical surface. This approach was proposed in RSN MRI by Yeo et al., 2011 and yielded the $N_\upsilon \times 1175$ reduced connectivity array P, defined as follows:

$$P = \overline{CC}_{1175}^T, \quad (5)$$

where $T$ denotes matrix transpose.

**5.** Compensation for MEG-imaging resolution and sensitivity: To minimize the influence of the uneven sensitivity of MEG source imaging to anatomical features (source orientation and depth), the previous steps were applied to surrogate MEG sensor data (independent and identically distributed, zero-mean, unit variance Gaussian sensor time series of same length as the original data's, for 12 surrogate individual data). The corresponding pairwise reduced connectivity array for surrogate data was obtained and denoted $\tilde{P}$. From the singular value decomposition (SVD) of $\tilde{P}$, $\tilde{P} = \tilde{U}\ S\ \tilde{V}^T$, the first spatial singular mode in $\tilde{U}$ was used to create $\tilde{\Pi}$, the orthogonal projector away from the principal mode of spurious connectivity due to MEG-imaging resolution and uneven sensitivity.

**6.** RSN maps as principal modes of connectivity: The RSN maps were defined as the principal spatial modes of P after they were corrected using the $P\tilde{\Pi}$ projector (see previous step), and identified as U, obtained from the following SVD:

$$P\tilde{\Pi} = USV^T. \quad (6)$$

Figure 3 shows the cortical maps thresholded at 40% of their maximum value and a minimum 2.5 cm$^2$ cluster size, of 5 principal spatial modes of the signal CSM projected away from the principal noise CSM pattern.

The extracted network across all subjects of the megPAC and the alternative models, which corresponded best to the DMN, were compared in Figure 4b. We used the default-mode map as shown in the lower right part of Figure 3 as documented in Vincent et al., 2008 to test for the correspondence between the DMN map and the maps based on the models. We calculated the ratio of correctly detected DMN areas versus false positively detected areas. The ratios for the models were compared with students t-test and subsequent Bonferroni correction. The ratio allows for estimating the correspondence in the spatial domain.

For each seed location $l$, the z-scored connectivity pattern of the seed region (i.e., the $l^{th}$ row of $\bar{C}$, standardized with respect to the mean and standard deviations observed with surrogate time series at the same location $l$) was obtained. All other brain locations were labeled according to the maximum observed connectivity z-score amongst the seed candidate region. Only regions with z-scores above 7 were considered for labeling. This method was used to generate Figure 4a, where seeds of interest were positioned in 3 distinct longitudinal aspects of the inferior frontal gyrus.

All maps were spatially-interpolated onto a higher-resolution version of the template brain, with 120,000 vertices, using the procedure available in Brainstorm.

## 3 Results

### Ubiquitous Phase-Amplitude Coupling across the Human Cortex

We first tested whether physiologically relevant PAC can be detected globally from human brain dynamics during rest. To this end, we performed source imaging (Baillet, Mosher, and Leahy, 2001; Tadel et al., 2011) from the MEG recordings. At every cortical location, the direct PAC measure (Özkurt and Schnitzler, 2011) was computed between the low-frequency phase and high-frequency amplitude of oscillatory MEG source signals. Multiple candidate low-frequency components for phase were tested between 2 to 12 Hz in bins of 0.5 Hz and from 12 to 48 Hz in 2 Hz steps. The reason for testing systematically a wide range of low-frequency components is the lack of consensus across previous published findings about a preferred band of low-frequency oscillations for phase coupling with high-gamma amplitude bursts. Phase-locked high-frequency amplitude fluctuations were tested in the higher gamma frequency range (80-150 Hz). For every source, direct PAC scores were obtained for each tested pair of low-frequency phase and high-frequency amplitude. We then determined the frequency pair with the highest direct PAC score and assessed statistical significance.

For the highest PAC score reported here 41%–61% of the sources at the individual level showed significant PAC ($p < 0.05$, Methods). The main modes across subjects of the low-frequency phase components were prominently in the delta (2-4 Hz) (65.3% of the cortical surface area averaged across subjects, with 18.6–34.8% IIR) and theta (4-8 Hz) bands (33.7% of the cortical surface area averaged across subjects, with 14.3–20.0% IIR). The alpha (8-12 Hz) band was found as low-frequency phase component over 1% (3.9–7.8% IIR) of the cortex. Low-frequency phase components in the beta band (12-30 Hz) remained spatially marginal (0% on average, with 0.1–10.3% IIR). No significant PAC with low-frequency phase in the low-gamma range (30-48 Hz) was found. Figure 2a shows the low frequency phase of the PAC averaged across subjects. For this average the low frequency phase of the maximal and significant PAC was used. Note that no spatial pattern was found in these results. It rather demonstrates that delta and theta are the main low-frequency phases. Having identified PAC over the whole brain suggests that it is not confined to certain brain regions, but may represent a fundamental building block for communication within the brain.

To ensure that the maximal PAC is not driven by the power of the low-frequency phase we determined the difference in frequency of the low-frequency phase from the maximal PAC and the frequency corresponding to the maximal power. In 80% of all sources across subjects these two frequencies were at least 1Hz apart and in 69% at least 2Hz.

To provide an illustrative example of the phase-amplitude coupling, we used an event-related average of spectrograms of ongoing cortical signals obtained about the troughs of the dominant low-frequency phase component. This approach is similar to the one of Canolty et al., 2006. These results are shown for arbitrarily chosen brain locations of one subject in Figure 2b. We found significant levels of temporal correlation ($p < 0.05$, Methods) between the amplitude fluctuations of high-gamma activity and the phase cycles of local low-frequency oscillations.

## Phase-Amplitude Coupling and Resting-State Networks

We tested the second hypothesis that the ongoing dynamics of local PAC oscillations determine network formation between the nodes of RSN.

In order to capture the most salient features of ongoing local PAC dynamics from ongoing MEG source time series, a signal transform was applied at each cortical location: The amplitude of high-gamma (80-150 Hz) bursts was linearly interpolated between the troughs and peaks of the low-frequency phase cycles with highest PAC to high-frequency amplitude. In essence, the interpolation of the peaks and troughs reduces the original MEG source time series to the peaks and troughs of optimal PAC cycles, which are key timing events for long-range communication. In local field potential recordings, the convention is that these key events occur at the troughs of the low-frequency phase (Buzsáki and Draguhn, 2004; Canolty et al., 2006). However, MEG source estimation detects current flows, not electrical potentials, and presents a $\pm\pi$ phase ambiguity, which depends on conventional default orientation of elementary current dipole sources constrained to the local cortical anatomy (Baillet, Mosher, and Leahy, 2001). Hence we considered both peaks and troughs as phase events of interest. We called the resulting sub-sampled signal model "megPAC".

megPAC signals were obtained for each individual subject and processed for RSN extraction (Methods). Figure 3 shows that the principal spatial modes of resting-state connectivity obtained with the megPAC signal model **show similarities** to the typical RSN reported by fMRI studies.

Our results therefore confirm that RSN are determined by correlated dynamics of local PAC fluctuations between regional nodes.

We further tested whether more fine-grained and anatomy-specific analysis of functional connections in the brain can be detected from the megPAC model with a seed-based analysis. Anatomical seeds were placed in the orbitalis (IFGor), triangularis (IFGtr), and opercularis (IFGop) aspects of the left inferior frontal gyrus. The functional connectivity patterns obtained were strikingly similar to those reported from diffusion-weighted MRI tractography studies and post-mortem dissections (Catani et al., 2012) (Figure 4a): Connections with IFGtr were circumscribed about the middle lateral frontal and central regions. Connections with IFGop extended to the pre-supplementary motor area (SMA), anterior and middle cingulate regions, the insula, the mouth sensori-motor cortex, and the superior and middle temporal lobe.

## Validation of the signal models

We quantified the correspondence of the resting-state networks identified from using the megPAC model and the three alternative models described in the methods with a natural benchmark, using a standard DMN map from fMRI (Vincent et al., 2008). We calculated the ratio of the percentage correspondence versus percentage falsely identified DMN regions for each signal model. Only the megPAC model shows a ratio larger than 1, indicating that it correctly identified a higher percentage of actual DMN regions as belonging to the DMN than non-DMN regions. Therefore the megPAC model yielded a significantly higher correspondence to the DMN than all other tested models (Figure 4b, $p < 0.001$). Furthermore

the megPAC model with theta only and the megPAC model with random troughs yielded a lower correspondence for the DMN than the megPAC model from random data. This clearly indicates that only the megPAC model properly captures the dynamics of the resting state. For the DMN, medial prefrontal regions, the anterior temporal lobe, posterior cingulate cortex (PCC), and the left and right inferior parietal lobules are the main components found with resting-state fMRI. Our analysis essentially revealed the prefrontal aspects of the DMN, with no identified contribution from the PCC and inferior parietal regions. Note that the PCC's contribution to the DMN was also not detected in previous MEG studies of the RSN using data-driven techniques (Brookes et al., 2011).

We calculated the ratio of corresponding to non-corresponding identified regions for the DAN, the visual network, and the right fronto-parietal network. We used the standard maps shown in figure 3 (Vincent et al., 2008; Yeo et al., 2011) and found that this ratio was 1.88 for the DAN, 0.03 for the visual network, and 3.38 for the right fronto-parietal network. The low correspondence for the visual network might be due to the smaller spatial extension of the MEG-based network. The MEG analysis detected an additional medial frontal component, which is not a typical part of the fMRI-based visual network. A combination of the DAN and the sensorimotor network (SMN) was detected with MEG. This is in accordance with seed-based analysis in fMRI data (Vincent et al., 2008) where the DAN/SMN is also extracted when placing a seed in the superior parietal lobule and the middle temporal area (MT+). For the right fronto-parietal network, the same lateral components as with fMRI were detected (prefrontal cortex, inferior parietal lobule, and inferior temporal gyrus). Yeo et al. (2011) described additional medial components for the fronto-parietal network, which were not detected with MEG. Concerning the auditory network, a clear activation of the left auditory cortex as well as the inferior frontal gyrus was detected with MEG, while the activation of the right auditory cortex was missing.

## 4 Discussion

In the present study we demonstrated that phase-amplitude coupling provides a mechanism for brain network formation, which reconciles previous findings and theories on long-range communication between neural populations.

Our first result is that local PAC can be demonstrated during rest over the whole cortex and that it is accessible non-invasively in humans. In particular, we found cortical PAC of ongoing, local activity between a slower low-frequency phase (predominantly in the 2-12Hz range) and bursts of high-frequency activity (80Hz and above) at the peaks and/or the troughs of the low-frequency oscillations. These results obtained with MEG source imaging extend previous reports obtained with invasive recording techniques and restricted to a limited number of brain regions (Canolty et al., 2006; Tort et al., 2008, 2009; Voytek et al., 2010). Thus, a comprehensive map of PAC measures over the entire cortical surface was obtained in each tested healthy subject. These results provide a promising avenue for systematically studying PAC and its relevance for neural communication in other conditions than rest.

Second, we showed that PAC mechanisms contribute to long-range neural communication between brain regions in the resting-state. For this purpose, we identified the principal modes of connectivity from the correlated fluctuations of a signal model based on local dynamics of phase-amplitude coupling (megPAC). Through the specific sampling of the gamma-amplitude with the restriction to the peaks and troughs of the low frequency, it was ensured that both features of the PAC were represented in the model. Furthermore only if two brain regions have the same low-frequency-phase and gamma amplitude, will the correlation be high. Thereby the connectivity maps reveal brain regions with the same PAC characteristics. The megPAC model revealed the expected major resting-state networks and was corroborated with a seed-based approach. The correspondence to a standard default map was demonstrated through statistical comparison of corresponding and non-corresponding detected regions. Most of the missing regions are within the medial aspects of the cortical hemispheres, which might be due to the lower sensitivity of MEG within these regions. We do not have the individual resting state fMRI maps and therefore a direct comparison was not possible.

This result shows that it is possible to identify motifs of megPAC signal correlation that are compatible with known, finer anatomical connections (Catani et al., 2012). Taken together, our results suggest that phase-amplitude coupling is an important component of the electrophysiology underlying network generation in the resting-state

Furthermore, our results reconcile observations from previous resting-state MEG studies in humans (Brookes et al., 2011; Pasquale et al., 2010) and combined BOLD and electro-physiology recordings in animals (Logothetis et al., 2001). They demonstrate that both the lower-frequency components reported by these MEG studies and the high-frequency oscillations found in invasive recordings are actually coupled and that they both contribute to a unifying mechanism of resting-state brain connectivity.

The fact that resting-state networks are accessible non-invasively using MEG opens new and substantial methodological possibilities for investigating the dynamics of resting-state activity at multiple temporal and spatial scales. In particular, using the time resolution of MEG and our approach for the analysis of resting-state activity, it is in principle now possible to study the dynamical interplay between resting-state networks occurring at a finer time scale. We anticipate these results will stimulate further research on the physiology of the cerebral resting-state, its transition in response to stimuli and during task performance, and will ultimately contribute to finding new markers of healthy and diseased brain function.

### Neural Network Formation with Synchronized Gating

Based on our findings here and previous studies, we propose the model of *synchronized gating* (SG). SG extends two previously proposed hypotheses for large-scale neural communication: the *communication-through-coherence* (CTC) hypothesis (Fries, 2005) and the *binding-by-synchronization* (BBS) model (Singer, 1999; Varela et al., 2001). The idea of the synchronized gating model is that the synchronized phase of slower neural oscillations provides a common gating mechanism between multiple brain regions: the low-frequency phase time-marks the occurrence of coherent, local high-frequency activity, which comprises regional post-synaptic integration and spiking activity. Underlying this model is

the previously documented finding that slower oscillatory rhythms time-mark the operations of local circuits (Buzsáki and Wang, 2012). In addition, low-frequency oscillations have been reported to coordinate long-range communication, while gamma oscillations (40-150 Hz) coordinate local communication (Buzsáki and Draguhn, 2004; Stein, Chiang, and König, 2000). If low-frequency phases are asynchronous (e.g., occurring at different frequencies and/or with a phase delay), the "gate is closed", coherent high-frequency oscillations and/or synchronous cell firing are less likely to occur, and communication/ coactivation between two brain regions is suboptimal.

Experimental evidence supported by computational models (Vicente et al., 2008) demonstrates that precise synchronization of neural oscillations can emerge with zero time lag to form networks. This is achieved through cortical (Buzsáki and Wang, 2012; Hipp et al., 2012) or subcortical (Sherman and Guillery, 2002) hubs, which act as dynamical relays of long-distance cortico-cortical communication. This network architecture circumvents the influence of variable axonal lengths and conduction delays on time lags between neural signals (Vicente et al., 2008). Thereby, according to SG, the recruitment of regions to participate in networks becomes a dynamic and flexible process, because the recruitment is not conditioned to direct connections between network nodes. The flexibility in network formation proposed by the SG model could therefore be essential for behavioral adaptation and promote developmental and learning abilities.

In summary, network formation by SG requires that nodal regions demonstrate synchronized low-frequency activity with no phase delay, which regulates the occurrence of coherent levels of local high-frequency bursts. In essence, it encapsulates the essence of both the CTC and BBS hypotheses in a single proposition. Figure 5 illustrates the basic mechanisms posited by the SG model.

### Methodological Considerations

We have used the phase-amplitude coupling measure, which has been proposed before and yielded the most robust results. Still, there are known methodological pitfalls with any PAC measure. The first one relates to the phase-ambiguity in MEG signals. In particular, it remains to be clarified whether the high frequency bursts occur preferentially at the trough, as suggested by Canolty et al., 2006, or another phase of the low-frequency cycle.

The second methodological pitfall concerns the sensitivity to low-frequency phase components with asymmetric cycles, as reported by local recordings (Buzsáki and Draguhn, 2004: Haider et al., 2006; Steriade et al., 1996). Related to this edges in the data lead to artificial PAC (Kramer, Tort, and Kopell, 2008).

Still PAC has been found in numerous studies using ECoG, LFP, and MEG data (Canolty et al., 2006; Özkurt et al., 2011; Tort et al., 2008) making it unlikely that PAC is artefactual. Moreover, our particular exemplary maps in Figure 2b show the averaged low-frequency signal. In this average no asymmetry of the oscillation is seen, therefore indicating that our results are not driven by spurious phase asymmetry. Furthermore our choice for chirplet time-frequency decompositions yielded a good combination for time and frequency resolution.

The third methodological issue related to PAC is that it could potentially be driven by the low-frequency with the maximal power. Our results indicate that this is not the main driving cause of the PAC, because in 80% of all subjects these two frequencies did not align with one another. This also suggests a possible alternative mechanism for the electrophysiological origins of resting-state networks than proposed in previous MEG studies (Brookes et al., 2011; Hipp et al., 2012; Pasquale et al., 2010).

In summary, we established that local phase-amplitude coupling between neural oscillations is a fundamental mechanism for long-range communication between brain regions. With a signal model based on phase-amplitude coupling, resting-state networks could be extracted. Based on these results, we suggested the synchronized gating hypothesis as a mechanism enabling long-range neural communication and functional connectivity in the brain, during rest and task performance.

## A Chirplet transform

Chirplets separate a time series not only in its time and frequency components, but also allow to consider a shear in time and frequency as well as a time dilation/frequency contraction. To construct a chirplet a windowing function such as a Gaussian window is applied to a chirp. Therefore in the case of a Gaussian windowing function, which has been used in the present paper, the chirplet is described as follows:

$$g(t) = \frac{1}{\sqrt{\sqrt{\pi}\Delta_t}} e^{-\frac{1}{4}\left(\frac{t-t_c}{\Delta_t}\right)^2} e^{j2\pi[c(t-t_c)^2 + f_c(t-t_c)]} \tag{7}$$

$t_c$ is the time center, $f_c$ the frequency center, $\Delta_t$ the duration, and c the chirprate of the chirplet. In the present paper the chirprate was set to 0. These parameters give a greater flexibility in covering the time-frequency domain. For an in depth review see Mann and Haykin, 1995.

## Acknowledgments

## References

Baillet S, Mosher J, Leahy R. Electromagnetic brain mapping. IEEE Signal Processing Magazine. 2001; 18(6):14–30.

Biswal BB, et al. Toward discovery science of human brain function. Proc Natl Acad Sci U S A. 2010; 107:4734–4739. [PubMed: 20176931]

Brookes MJ, Woolrich M, Luckhoo H, Price D, Hale JR, Stephenson MC, Barnes GR, Smith SM, Morris PG. Investigating the electrophysiological basis of resting state networks using

magnetoencephalography. Proc Natl Acad Sci U S A. 2011; 108:16783–16788. [PubMed: 21930901]

Buckner RL, Snyder AZ, Shannon BJ, LaRossa G, Sachs R, Fotenos AF, Sheline YI, Klunk WE, Mathis CA, Morris JC, Mintun MA. Molecular, structural, and functional characterization of Alzheimer's disease: evidence for a relationship between default activity, amyloid, and memory. J Neurosci. 2005; 25:7709–7717. [PubMed: 16120771]

Buzsáki G, Draguhn A. Neuronal oscillations in cortical networks. Science. 2004; 304:1926–1929. [PubMed: 15218136]

Buzsáki G, Wang XJ. Mechanisms of gamma oscillations. Annu Rev Neurosci. 2012; 35:203–225. [PubMed: 22443509]

Canolty RT, Edwards E, Dalai SS, Soltani M, Nagarajan SS, Kirsch HE, Berger MS, Barbara NM, Knight RT. High gamma power is phase-locked to theta oscillations in human neocortex. Science. 2006; 313:1626–1628. [PubMed: 16973878]

Canolty RT, Knight RT. The functional role of cross-frequency coupling. Trends Cogn Sci. 2010; 14:506–515. [PubMed: 20932795]

Catani M, Dell'Pacqua F, Vergani F, Malik F, Hodge H, Roy P, Valabregue R, Thiebaut de Schotten M. Short frontal lobe connections of the human brain. Cortex. 2012; 48:273–291. [PubMed: 22209688]

Fries P. A mechanism for cognitive dynamics: neuronal communication through neuronal coherence. Trends Cogn Sci. 2005; 9:474–480. [PubMed: 16150631]

Haider B, Duque A, Hasenstaub AR, McCormick DA. Neocortical network activity in vivo is generated through a dynamic balance of excitation and inhibition. J Neurosci. 2006; 26:4535–4545. [PubMed: 16641233]

Hipp JF, Hawellek DJ, Corbetta M, Siegel M, Engel AK. Large-scale cortical correlation structure of spontaneous oscillatory activity. Nat Neurosci. 2012; 15:884–890. [PubMed: 22561454]

Huang MX, Mosher JC, Leahy RM. A sensor-weighted overlapping-sphere head model and exhaustive head model comparison for MEG. Phys Med Biol. 1999; 44:423–440. [PubMed: 10070792]

Jensen O, Colgin LL. Cross-frequency coupling between neuronal oscillations. Trends Cogn Sci. 2007; 11:267–269. [PubMed: 17548233]

Kasdin N. Discrete Simulation of Colored Noise and Stochastic Processes and $1/f^{\alpha}$ Power Law Noise Generation. Proceedings of the IEEE. 1995; 83:802–827.

Kramer MA, Tort ABL, Kopell NJ. Sharp edge artifacts and spurious coupling in EEG frequency comodulation measures. J Neurosci Methods. 2008; 170:352–357. [PubMed: 18328571]

Lakatos P, Shah AS, Knuth KH, Ulbert I, Karmos G, Schroeder CE. An oscillatory hierarchy controlling neuronal excitability and stimulus processing in the auditory cortex. J Neurophysiol. 2005; 94:1904–1911. [PubMed: 15901760]

Leopold DA, Maier A. Ongoing physiological processes in the cerebral cortex. Neuroimage. 2012; 62:2190–2200. [PubMed: 22040739]

Logothetis NK, Pauls J, Augath M, Trinath T, Oeltermann A. Neuro-physiological investigation of the basis of the fMRI signal. Nature. 2001; 412:150–157. [PubMed: 11449264]

Mann S, Haykin S. The chirplet transform: A generalization of Gabor's logon transform. Vision Interface. 1991; 91:3–7.

Mann S, Haykin S. The Chirplet Transform: Physial Considerations. IEEE Transactions on Signal Processing. 1995; 43:2745–2761.

Newey WK, West KD. A Simple, Positive Semi-definite, Heteroskedasticity and Autocorrelation Consistent Covariance Matrix. Econometrica. 1987; 55:703–708.

Nolte G, Curio G. The effect of artifact rejection by signal-space projection on source localization accuracy in MEG measurements. IEEE Trans Biomed Eng. 1999; 46:400–408. [PubMed: 10217878]

Osipova D, Hermes D, Jensen O. Gamma power is phase-locked to posterior alpha activity. PLoS One. 2008; 3:e3990. [PubMed: 19098986]

Özkurt TE, Butz M, Homburger M, Elben S, Vesper J, Wojtecki L, Schnitzler A. High frequency oscillations in the subthalamic nucleus: a neurophysiological marker of the motor state in Parkinson's disease. Exp Neurol. 2011; 229:324–331. [PubMed: 21376039]

Ozkurt TE, Schnitzler A. A critical note on the definition of phase-amplitude cross-frequency coupling. J Neurosci Methods. 2011; 201:438–443. [PubMed: 21871489]

Pasquale F, de Penna SD, Snyder AZ, Lewis C, Mantini D, Marzetti L, Belar-dinelli P, Ciancetta L, Pizzella V, Romani GL, Corbetta M. Temporal dynamics of spontaneous MEG activity in brain networks. Proc Natl Acad Sci USA. 2010; 107:6040–6045. [PubMed: 20304792]

Raichle ME. The restless brain. Brain Connect. 2011; 1:3–12. [PubMed: 22432951]

Rivière D, Geffroy D, Denghien I, Souedet N, Cointepas Y. BrainVISA: an extensible software environment for sharing multimodal neuroimaging data and processing tools. Proceedings of 15th Conference of the Human Brain Mapping Society. 2009

Sherman SM, Guillery RW. The role of the thalamus in the flow of information to the cortex. Philos Trans R Soc Lond B Biol Sci. 2002; 357:1695–1708. [PubMed: 12626004]

Shmuel A, Leopold DA. Neuronal correlates of spontaneous fluctuations in fMRI signals in monkey visual cortex: implications for functional connectivity at rest. Hum Brain Mapp. 2008; 29(7):751–761. [PubMed: 18465799]

Singer W. Neuronal synchrony: a versatile code for the definition of relations? Neuron. 1999; 24:49–65. 111–25. [PubMed: 10677026]

Smith K. Neuroscience: Idle minds. Nature. 2012; 489:356–358. [PubMed: 22996531]

Smith SM, Fox PT, Miller KL, Glahn DC, Fox PM, Mackay CE, Filippini N, Watkins KE, Toro R, Laird AR, Beckmann CF. Correspondence of the brain's functional architecture during activation and rest. Proc Natl Acad Sci USA. 2009; 106:13040–13045. [PubMed: 19620724]

Stein A, von Chiang C, König P. Top-down processing mediated by interareal synchronization. Proc Natl Acad Sci U S A. 2000; 97:14748–14753. [PubMed: 11121074]

Steriade M, Contreras D, Amzica F, Timofeev I. Synchronization of fast (30-40 Hz) spontaneous oscillations in intrathalamic and thalamocortical networks. J Neurosci. 1996; 16:2788–2808. [PubMed: 8786454]

Tadel F, Baillet S, Mosher JC, Pantazis D, Leahy RM. Brainstorm: A User-Friendly Application for MEG/EEG Analysis. Computational Intelligence and Neuroscience. 2011; 2011:13.

Taulu S, Kajola M, Simola J. Suppression of interference and artifacts by the Signal Space Separation Method. Brain Topogr. 2004; 16:269–275. [PubMed: 15379226]

Tomasi D, Volkow ND. Abnormal functional connectivity in children with attention-deficit/hyperactivity disorder. Biol Psychiatry. 2012; 71:443–450. [PubMed: 22153589]

Tort ABL, Kramer MA, Thorn C, Gibson DJ, Kubota Y, Graybiel AM, Kopell NJ. Dynamic cross-frequency couplings of local field potential oscillations in rat striatum and hippocampus during performance of a T-maze task. Proc Natl Acad Sci U S A. 2008; 105:20517–20522. [PubMed: 19074268]

Tort ABL, Komorowski RW, Manns JR, Kopell NJ, Eichenbaum H. Theta-gamma coupling increases during the learning of item-context associations. Proc Natl Acad Sci U S A. 2009; 106:20942–20947. [PubMed: 19934062]

Varela F, Lachaux JP, Rodriguez E, Martinerie J. The brainweb: Phase synchronization and large-scale integration. Nature Reviews Neuroscience. 2001; 2:229–239.

Vicente R, Gollo LL, Mirasso CR, Fischer L, Pipa G. Dynamical relaying can yield zero time lag neuronal synchrony despite long conduction delays. Proc Natl Acad Sci U S A. 2008; 105:17157–17162. [PubMed: 18957544]

Vincent JL, Kahn L, Snyder AZ, Raichle ME, Buckner RL. Evidence for a frontoparietal control system revealed by intrinsic functional connectivity. J Neurophysiol. 2008; 100:3328–3342. [PubMed: 18799601]

Voytek B, Canolty RT, Shestyuk A, Crone NE, Parvizi J, Knight RT. Shifts in gamma phase-amplitude coupling frequency from theta to alpha over posterior cortex during visual tasks. Front Hum Neurosci. 2010; 4:191. [PubMed: 21060716]

Weisend, M.; Hanlon, F.; Montaño, R.; Ahlfors, S.; Leuthold, A.; Pantazis, D.; Mosher, J.; Georgopoulos, A.; Hämäläinen, M.; Aine, C. Paving the way for cross-site pooling of

magnetoencephalography (MEG) data. International Congress Series 1300. New Frontiers in Biomagnetism. Proceedings of the 15th International Conference on Biomagnetism; Vancouver, BC, Canada. August 21-25, 2006; 2007. p. 615-618.

Yeo BTT, Krienen FM, Sepulcre J, Sabuncu MR, Lashkari D, Hollinshead M, Roffman JL, Smoller JW, Zöllei L, Polimeni JR, Fischl B, Liu H, Buckner RL. The organization of the human cerebral cortex estimated by intrinsic functional connectivity. J Neurophysiol. 2011; 106:1125–1165. [PubMed: 21653723]

## Highlights

- Propose and experimentally verify synchronized gating as mechanism for communication.

- Non-invasive detection across the entire cortex of local phase-amplitude coupling.

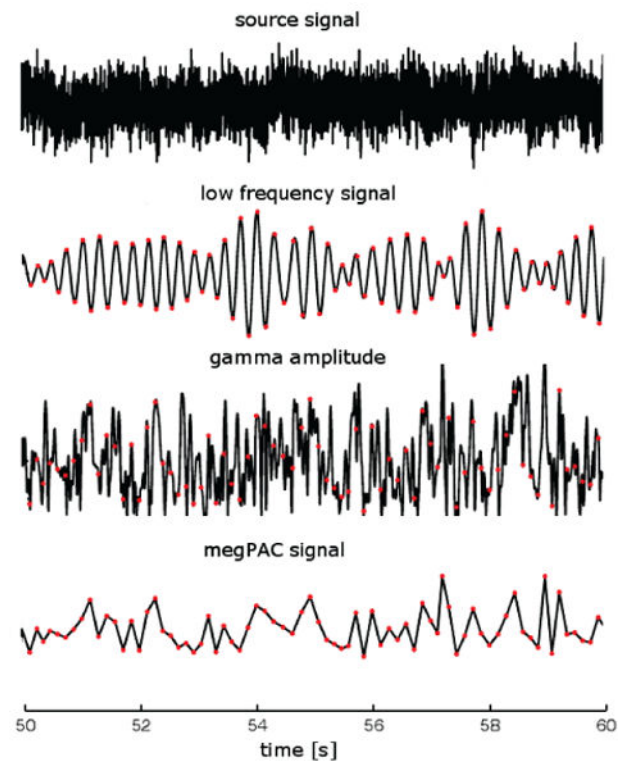- Spatial modes of cross-frequency coupling correspond to resting-state networks.

**Figure 1. Generation of the megPAC model**
Starting from each cortical MEG source time series (top row): 1) the troughs and peaks of the optimal low-frequency phase were determined from the original sources signal (second row); 2) the amplitude of the same source signal in the [80,150] Hz gamma range was extracted (third row). For the megPAC model, the gamma amplitude values at the troughs and peaks of the low-frequency were linearly interpolated (fourth row).
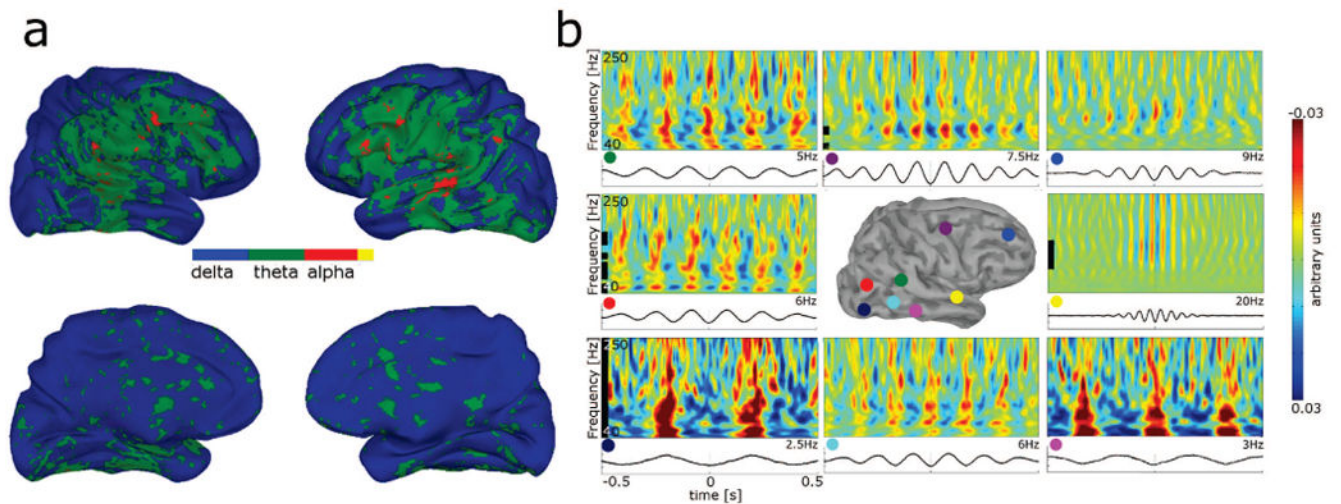
**Figure 2. Ubiquitous Phase-Amplitude Coupling in the Human Cortex**

(a): Average low frequency component for PAC phase, following anatomical co-registration of individual cortical surfaces ($n = 12$) to a template brain. (b): Representative spectrograms of ongoing cortical activity averaged at the phase troughs of the low frequency with the highest PAC at each tested brain location in 1 representative subject. The scales are [-0.5, 0.5] s (x-axis), and [40, 250] Hz (y-axis). The tested cortical locations are shown with colored dots on the individual's brain surface, with color correspondence with the time-frequency maps (shown at lower left corner). The spectrograms and ongoing cortical signals were averaged about the troughs of the optimal low-frequency oscillations for phase. At each cortical location, the resulting event-related average of the raw source signal is shown, with the value of the corresponding frequency for phase in the lower sub-panel of each plot. The color bar immediately to the left of the time-frequency maps indicates significant correlation ($p < 0.05$, negative in red, positive in black) between the amplitude modulations of high-frequency oscillations and the event-related average of the raw signal.
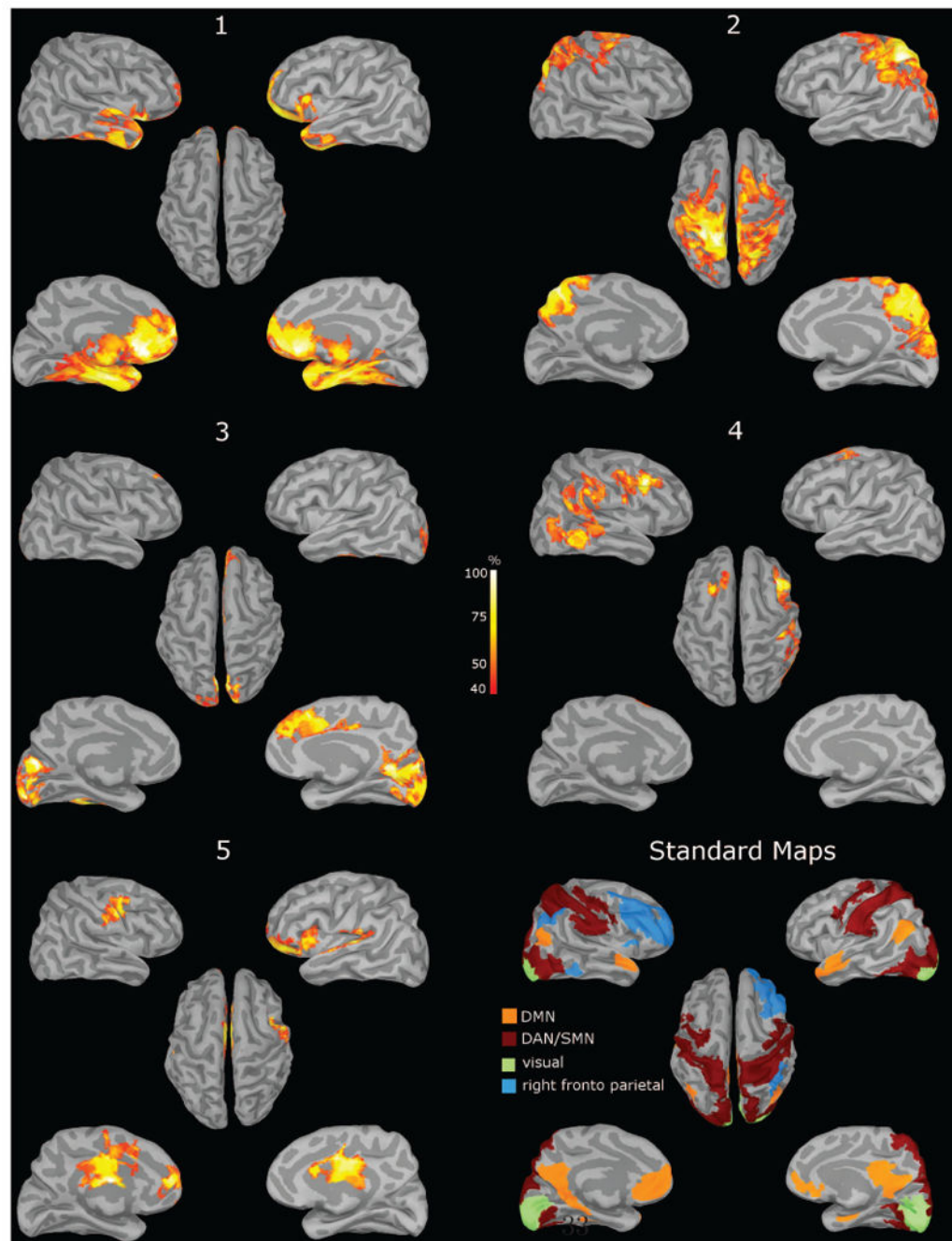
**Figure 3. Group Modes and Patterns of Resting-State Connectivity**
The anatomy of the resting-state networks revealed by the megPAC signal model based on phase-amplitude coupling mechanisms between neural ensembles is similar to those typically found using hemodynamic imaging techniques. **Five principal spatial modes of connectivity from the megPAC signal model are displayed. For comparison the default-mode network (DMN), dorsal attention network combined with sensorimotor network (DAN/SMN), visual network, and right fronto-parietal network are shown**

**based on fMRI results, as provided in Vincent et al., 2008 and Yeo et al., 2011. For the first four MEG networks there is an overlap to these four fMRI networks.**
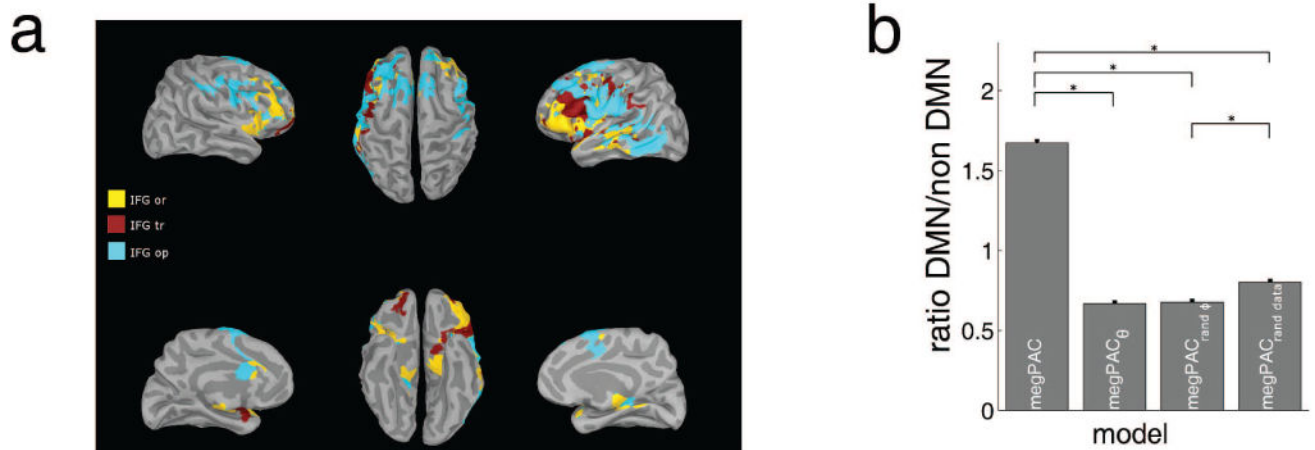
**Figure 4.**
(a) The frontal lobe connections identified from the megPAC time series are consistent with results from MRI tractography and post-mortem dissection techniques (Catani et al., 2012). (b) The ratio of the average pairwise signal correlation between regions within the DMN over the pairwise correlation between brain regions outside the DMN was computed for the megPAC, the megPAC model with the low-frequency fixed at 5.4 Hz, the megPAC model with random events for the low-frequency and the megPAC model from random data. The regions of interest within the DMN are shown in figure 3 and were selected based on Vincent et al., 2008. Overall the megPAC model yielded the highest correspondence with the DMN (*: $p < 0.001$).
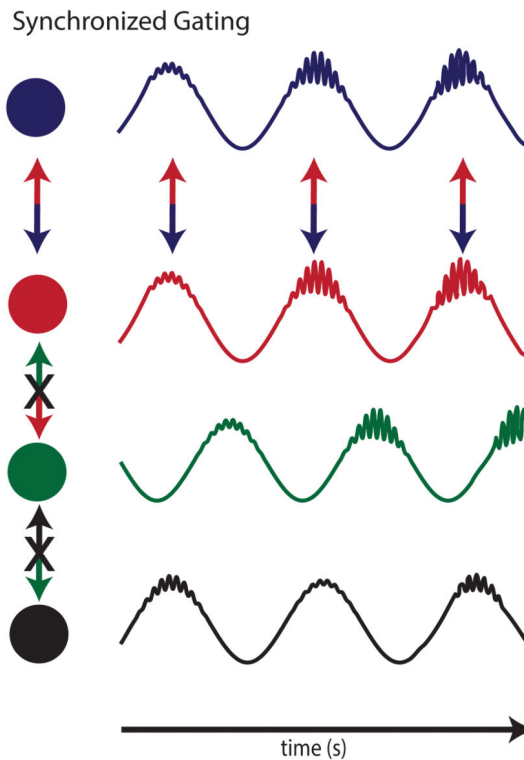
**Figure 5.**
Principles of *Synchronized Gating* (SG) for long-range neural communication. The colored dots represent neuronal populations; the connecting arrows indicate when two neuronal groups can communicate. When crossed out, this indicates that neural communication cannot occur. In the present example, only the red and blue neuronal groups communicate with each other: The respective phase of the local low-frequency oscillatory activity are synchronized and therefore provide the necessary gating mechanism for long-range communication between the two groups. In addition, the amplitudes of the high-frequency bursts are coherent, which indicates similar levels of local post-synaptic integration and spiking. Under the SG assumption, the green and black neuronal groups do not communicate with the other populations, because their low-frequency phase is not aligned or the local high-frequencies are not coherent with the red and blue populations, respectively. In contrast according to the CTC hypotheses, the black and blue neuronal group would communicate with each other.